

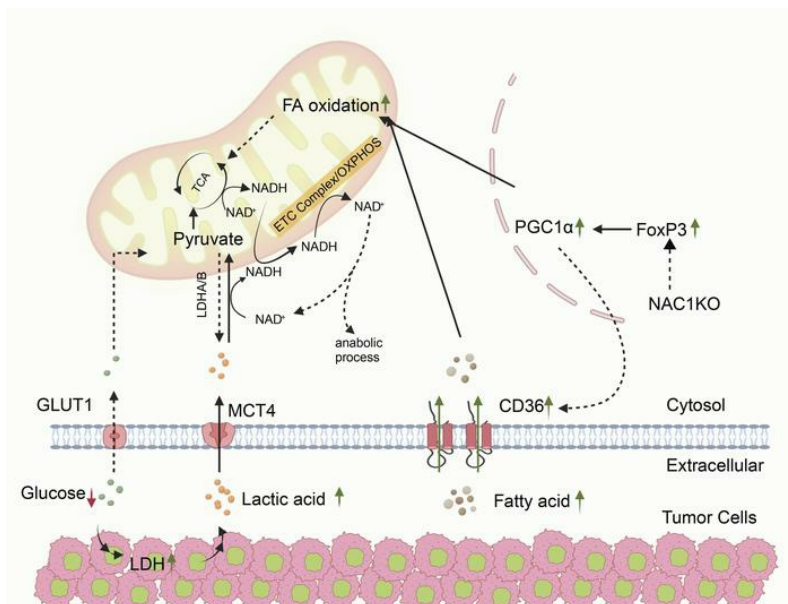
Metabolic Fitness of NAC1-Deficient Regulatory T Cells in the Tumor Microenvironment Fuels Tumor Growth

Anil Kumar, ... , Paul de Figueiredo, Jianxun Song

JCI Insight. 2025. <https://doi.org/10.1172/jci.insight.186000>.

Research In-Press Preview Immunology

Graphical abstract



Find the latest version:

<https://jci.me/186000/pdf>



31 **Abstract**

32 The nucleus accumbens-associated protein-1 (NAC1) has recently emerged as a pivotal factor in
33 oncogenesis by promoting glycolysis. Deletion of NAC1 in regulatory T cells (Tregs) has been
34 shown to enhance FoxP3 stability, a suppressor of glycolysis. This study delves into the intriguing
35 dual role of NAC1, uncovering that Tregs-specific deletion of NAC1 fosters metabolic fitness in
36 Tregs, thereby promoting tumorigenesis. Our results unveil that NAC1-deficient Tregs exhibit
37 prolonged survival and heightened function, particularly in acidic environments. Mechanistically,
38 we find that NAC1-deficient Tregs adapt to adverse conditions by upregulating FoxP3 expression,
39 engaging in CD36-mediated lipid metabolism, and enhancing PGC-1 α -regulated mitochondrial
40 function. In mouse tumor xenograft models, NAC1-deficient mice demonstrate increased
41 susceptibility to tumor growth. Notably, Tregs lacking NAC1 not only display elevated lipid
42 metabolism and mitochondrial fitness but also exhibit enhanced tumoral infiltration. Adoptive
43 Treg transfer experiments further underscore the supportive role of NAC1-deficient Tregs in tumor
44 growth. These findings suggest that modulating NAC1 expression in FoxP3⁺ Tregs could serve as
45 a promising approach to augment antitumor immunity. Understanding the intricate interplay
46 between NAC1 and Tregs opens avenues for potential therapeutic strategies targeting the tumor
47 microenvironment (TME).

48
49 **Keywords:** NAC1; Tregs; Cell metabolism; TME; Tumor growth

50 **Introduction**

51 Nucleus accumbens-1 (NAC1), a transcription co-factor associated with cancer, is a member of
52 the BTB/POZ (bric-a-brac tramtrack broad complex/poxvirus and zn-finger) family of nuclear
53 proteins. NAC1 overexpression is a feature of several cancer types including ovarian, cervical and
54 uterine cancers (1-3), and is believed to promote tumor initiation and progression (4, 5).
55 Furthermore, High expression of NAC1 is closely associated with recurrent ovarian serous
56 carcinoma and contributes to cancer drug resistance (6).

57 NAC1 is a critical regulator of glycolysis in ovarian cancer development through
58 stabilization of HIF-1 α , direct regulation of c-myc in tumor cells and subsequent regulation of
59 cellular metabolism (7). NAC1 enhances the expression of LDHA in tumor cells leading to higher
60 accumulation of lactic acid (LA) which resulted in altered cellular metabolism of cytotoxic T cells
61 (CTLs) in the tumor micro environment (TME) (8). It has been shown that T-cells can switch to
62 lactate uptake in a glucose starved TME. However, the reversal of the LDH reaction to generate
63 pyruvate drains the cellular NAD⁺ pools, effectively inhibiting GAPDH activity and glycolytic
64 flux. The nutrient deficient tumor environment along with LDHA mediated lactic acid production
65 create hostile condition for TILs leading to immune evasion (8-10). FoxP3⁺ regulatory T cells
66 (Tregs), a distinct and dynamic subset of CD4⁺ T cells, are an essential for maintenance of immune
67 cell homeostasis (11). Elevated levels of FoxP3⁺ Tregs within the tumor microenvironment (TME)
68 showed a positive correlation with poor prognosis in various cancer patients (12). Foxp3
69 reprograms T cell metabolism by suppressing c-myc and glycolysis, enhancing oxidative
70 phosphorylation, and increasing NAD oxidation (13). Foxp3 drives upregulation of components
71 of all the electron transport complexes, increasing their activity and ATP generation by oxidative
72 phosphorylation. These adaptations provide a survival and metabolic advantage to the Tregs over
73 effector T cells, by generating energy through FA metabolism (OXPHOS) in glucose deficient and

74 lactate rich TME (14-17). We recently reported that NAC1 acts as a negative regulator of FoxP3
75 in Tregs, and that NAC1-deficient (KO) mice are resistant to autoimmunity and exhibit strong
76 immunosuppressive activity as compared to wild-type (WT) mice (10). We show that NAC1 KO
77 mice generate higher frequency of CD4⁺ Tregs that exhibit a higher metabolic profile and immune
78 suppressive activity, increased acetylation and expression of FoxP3, and slower turnover of this
79 transcriptional factor (10). Because FoxP3⁺ Tregs are critically involved in tumor development and
80 progression *via* suppressing antitumor immunity and the elevated amount of FoxP3⁺ Tregs in
81 tumor microenvironment (TME) is positively correlated with poor prognosis in patients with
82 cancer (12), we intended to know whether and how NAC1-mediated control of Tregs and their
83 function impacts tumorigenesis. Our study found that Tregs with NAC1 deficiency are
84 metabolically more robust and functionally stronger than WT Tregs in TME, with upregulation of
85 the CD36 - PGC-1 α pathway and promotes tumor growth through increasing the infiltration of
86 FoxP3 Tregs to tumors. This FoxP3 and CD36 upregulation plays a pivotal role in supporting
87 enhanced lipid metabolism, mitochondrial fitness, and biogenesis within the tumor
88 microenvironment, all through a mechanism dependent on PGC-1 α . In adoptive Tregs transfer
89 experiment we confirmed that Treg specific NAC1 deficiency is sufficient to support tumor
90 initiation and growth. These results underscore the potential of targeting metabolic adaptation in
91 intratumoral Treg cells as a promising strategy for metabolic reprogramming of the TME.

92

93

94 **Results**

95 ***Syngeneic NAC1 KO mice are prone to tumor growth***

96 In our previous study, we reported the inhibitory role of NAC1 in FoxP3 expression within Tregs.
97 Given FoxP3's pivotal role in Treg function and its regulatory nexus with NAC1, we set out to
98 investigate whether NAC1 has any impact on tumor growth. To explore the role of NAC1 in tumor
99 development, we subcutaneously inoculated 3×10^6 B16-F10 or MC38 tumor cells into the right
100 flank of both wild-type (WT) and NAC1 knockout (NAC1 KO) mice, monitoring the progression
101 of the tumors. Remarkably, we observed that B16-F10 cells grew significantly faster and formed
102 larger tumors in NAC1 KO mice than in the age-matched WT mice (**Figure 1A**), leading to shorter
103 survival of the tumor-bearing mice (**Figure 1B**). We further examined tumor tissue sections
104 (**Figure 1C**) for lymphocyte infiltration using hematoxylin and eosin (H&E) staining (**Figure 1D**),
105 immunofluorescence staining (**Figure 1E**), and imaging mass cytometry (IMC) analysis (**Figure**
106 **1F, 1G**). H&E-stained tissue sections demonstrated an increased lymphocyte infiltration in the
107 MC38 tumors grown in NAC1 KO mice, as compared to that grown in WT animals (**Figure 1D**).
108 *t*-distributed stochastic neighbor embedding (*t*-SNE) plots of the imaging mass cytometry (IMC)
109 data confirmed that the total tumoral infiltration of FoxP3⁺ Tregs was significantly higher in NAC1
110 KO mice than that in WT mice, but the infiltration of total CD4⁺ T cells was significantly higher
111 in WT mice than in NAC1 KO mice (**Figure 1G**). Also, the infiltration of CD8⁺ and CD8⁺PD1⁺ T
112 cells was significantly higher in tumors grown in NAC1 KO mice than in tumors grown in WT
113 animals (**Figure 1G**), suggesting that exhaustion and reduced survival of CD8⁺ T cells may
114 contribute to the enhanced functional fitness of the tumor-infiltrating Tregs in NAC1 KO mice.

115

116 ***NAC1 negatively affects the survival and polarization of Tregs in acidic environments***

117 To demonstrate the effect of NAC1 on Tregs in harsh environment, we first compared the survival
118 of NAC1 KO Tregs with that of WT Tregs. CD4⁺CD25⁻ conventional T cells (Tconv) were isolated
119 from FOXP3-IRES-mRFP (FIR) reporter mice, cultured under polarizing conditions to generate
120 RFP⁺ induced Tregs (iTregs), and the optimal polarization efficiency was confirmed on various
121 days using flow cytometry (**Supplemental Figure 1A, 1B**). We also confirmed significant
122 difference of FoxP3 expression (**Supplemental Figure 1C**) in iTregs and similar IL-10
123 (**Supplemental Figure 1D**) and TGF- β (**Supplemental Figure 1E**) secretion profile in nTregs
124 and iTregs. Subsequently, we isolated CD4⁺CD25⁻ Tconv cells from both WT and NAC1 KO
125 mice, cultured them under identical polarizing conditions to generate iTregs. On day 5, WT and
126 NAC1 KO iTregs were cultured in media treated with 10 mM lactic acid (LA) or B16-F10
127 conditioned media (CM) for 48 hours. As NAC1 deficiency promotes FoxP3 expression (10), we
128 assessed FoxP3 expression in these cells. Notably, we observed that the untreated (70.1%), LA-
129 treated (72.2%), and CM-treated (75.1%) NAC1 KO iTregs displayed a higher polarization
130 efficiency than the untreated (57.0%), LA-treated (63.6%), and CM-treated (65.7%) WT iTregs
131 (**Figure 2A, 2B**). This observation aligns with the increased frequency of Tregs in the peripheral
132 tissues of NAC1 KO mice as compared to WT mice (10). We further examined whether expression
133 of NAC1 affects Treg proliferation. Using carboxyfluorescein succinimidyl ester (CFSE)-labeled
134 WT and NAC1 KO iTregs, we cultured them in LA-treated and CM-treated media and assessed
135 their proliferation using CFSE dilution assay. Interestingly, we found that the proliferation of both
136 WT and NAC1 KO iTregs was unaffected by LA treatment or CM treatment, suggesting that the
137 higher infiltration of Tregs in NAC1 KO mice is not associated with altered proliferation of Tregs
138 (**Figure 2E**). We also determined whether NAC1 deficiency has any effect on apoptosis, and found
139 that the untreated (15.6%), LA-treated (25.8%), and CM-treated (30.1%) NAC1 KO iTregs
140 exhibited significantly lower levels of apoptosis than the WT iTregs subjected to the same

141 treatment (22.0%, 37.1% and 45.7% respectively) (**Figure 2C, 2D**). These results indicate that
142 NAC1 KO iTregs are significantly less apoptotic and more resistant to the stress caused by acidic
143 environment and suggest that deficiency of NAC1 may promotes the survival of Tregs in the TME,
144 thereby increasing infiltration of Tregs to tumors.

145

146 ***Loss of NAC1 leads to enhanced functional activity of Tregs***

147 We next compared the functional activity of NAC1 KO Tregs with that of WT Tregs using an *ex-*
148 *vivo* suppression assay. In this assay, we stimulated the CFSE-labeled CD8⁺ effector T cells and
149 then co-cultured them in control media or CM with FACS-sorted Tregs isolated from the spleen
150 and lymph nodes (LN) of WT or NAC1 KO mice. The suppressive function was assessed by
151 analyzing CFSE dilution using flow cytometry. Our findings revealed that NAC1 KO Tregs were
152 significantly more suppressive compared to WT Tregs in both untreated and CM treated conditions
153 (**Figure 3A, 3B, Supplemental Figure 4A**). Further, the expression of Granzyme B (GzmB), an
154 enzyme that is highly expressed in tumor-infiltrating Tregs (18) and plays an important role in
155 increasing the metastatic burden in the lungs and eliminating conventional T cells in colorectal
156 cancer (19, 20), was significantly higher in NAC1 KO iTregs than in WT iTregs in the control
157 media, LA-containing media or CM (**Figure 3C, 3D, Supplemental Figure 3B**), suggesting that
158 GzmB is an important mediator of the suppressive capacity of NAC1 KO Tregs. Also, NAC1 KO
159 iTregs produced significantly higher amounts of suppressive cytokines, TGF- β and IL-10, than
160 WT iTregs, as evidenced by intracellular staining (**Figure 3E, 3F**). We also conducted
161 bioinformatics analysis in human tumor samples submitted in The Cancer Genome Atlas (TCGA)
162 database and we found that higher FoxP3 regulatory T cells are correlated with lower survival in
163 Kidney Renal Clear Cell Carcinoma (KIRC) (**Supplemental Figure 5A, 5B**) and Glioblastoma
164 Multiforme (GBM) (**Supplemental Figure 5C, 5D**). Furthermore, lower expression of NAC1 in

165 intra-tumoral Tregs also correlated with lower survival (**Supplemental Figure 5E**). These results
166 indicate that NAC1 has negative effects on the suppressive function of Tregs.

167

168 ***Loss of NAC1 results in upregulation of CD36 expression and elevation of lipid metabolism of***
169 ***Tregs in acidic environments.***

170 Since we observed that deletion of NAC1 prolonged the survival and enhanced the function of
171 Tregs under acidic condition (**Figure 2** and **Figure 3**) and NAC1 has a critical role in metabolic
172 reprogramming (3), we quired whether the effects of NAC1 on fitness and function of Tregs are
173 mediated through altered metabolism in Tregs. Because CD36, phagocytic receptor that mediates
174 fatty acid-induced metastasis via regulating fatty acid intake and metabolism, is selectively
175 upregulated in the intratumoral Tregs and functions as a central metabolic modulator that fine-
176 tunes mitochondrial fitness in lactic acid-rich TME (16, 21-23), we then examined the expression
177 of CD36 in the tumor-infiltrating Tregs. Tregs were isolated from the spleen (SPL), lymph nodes
178 (LN), and tumors of the B16-F10 melanoma bearing-NAC1 KO mice or WT mice, and the
179 expression of CD36 on WT and NAC1 KO iTregs was analyzed at 24 hours, 48 hours, and 72
180 hours following treatment with 10 mM of LA. Interestingly, NAC1 KO iTregs exhibited
181 significantly higher CD36 expression than WT iTregs at 48 hours (1.09% vs. 0.43%) and 72 hours
182 (3.79% vs. 1.16%) following the treatment, respectively, although the expression was similar at 24
183 hours after treatment. (**Supplemental Figure 2A, 2B**). Notably, tumor associated Tregs showed
184 significantly higher expression of CD36 than normal Tregs from the SPL and LN (**Supplemental**
185 **Figure 2C, 2D**). These results indicate that the deletion of NAC1 causes an increased CD36
186 expression under acidic conditions. Because NAC1 has a role in promoting expression of fatty
187 acid synthase (24) and CD36 participates in regulation of lipid metabolism (25), we next
188 determined whether the increased expression of CD36 in NAC1 KO Tregs was associated with

189 altered lipid metabolism. We examined lipid uptake through BODIPY FL C12 staining (BODIPY
190 500/510) and neutral lipid content through BODIPY (BODIPY 493/503) staining in iTregs treated
191 with LA or CM. Our experiments found a significantly higher level of neutral lipids in NAC1 KO
192 iTregs treated with CM than that in WT iTregs treated with CM, as evidenced by the staining of
193 BODIPY 493/503 (**Figure 4A**). Similarly, NAC1 KO iTregs internalized a significantly higher
194 amount of BODIPY 500/510 than WT iTregs under all the conditions (untreated, LA-treated, and
195 CM-treated (**Figure 4B**), with the most pronounced increase observed in the CM-treated cells
196 (**Figure 4C, 4D**). Furthermore, we analyzed the expression of the transcription coactivator
197 peroxisome proliferator-activated receptor gamma, coactivator 1 alpha (PPARGC1A, also known
198 as PGC-1 α), which is a master regulator of lipid metabolism and fatty acid transporters (such as
199 FAT/CD36 and FABP3). and mitochondrial biogenesis and coordinates with enhanced oxidative
200 phosphorylation and the electron transport chain (26, 27). Our analysis showed that compared with
201 the untreated, lactic acid-treated, or conditioned media-treated WT iTregs with NAC1 KO iTregs,
202 the level of PGC-1 α in the CM-treated NAC1 KO iTregs was significantly higher than that in the
203 corresponding WT iTregs, although both WT and NAC1 KO iTregs exhibited a significantly
204 increased PGC-1 α expression when treated with CM (**Figure 4E, 4F**). These results indicate that
205 NAC1 depletion is associated with increased PGC-1 α expression, CD36 expression, and enhanced
206 fatty acid transport and metabolism, rendering NAC1 KO Tregs metabolically more active and
207 better adapted to the environmental stress. These results demonstrate the role of NAC1 in
208 modulating Treg metabolism, especially in acidic environments, and imply the metabolic
209 adaptability of NAC1 KO Tregs in an unfavorable TME.

210

211 *Loss of NAC1 improves mitochondrial fitness of Tregs*

212 PGC-1 α is a key regulator of mitochondrial biogenesis and coordinates with enhanced oxidative
213 phosphorylation and the electron transport chain, playing a crucial role in cellular energy and
214 metabolism (26, 27). Our observation of the upregulated PGC-1 α and FoxP3 in NAC1 KO iTregs
215 prompted us to determine the effects of NAC1 deficiency on energy metabolism and mitochondrial
216 fitness in Tregs following LA or CM treatment. We found that mitochondrial respiration, as
217 indicated by the oxygen consumption rate (OCR) or oxidative phosphorylation (OXPHOS), was
218 significantly higher in NAC1 KO iTregs following treatment with LA or CM for 48 hours, as
219 analyzed by the mitochondrial stress test using oligomycin, FCCP and rotenone/antimycin A in a
220 Seahorse bioanalyzer (**Figure 5A**). We also examined different components of mitochondrial
221 respiration, including basal respiration, ATP-linked respiration, maximal respiration, and spare
222 respiratory capacity, which reflect mitochondrial and cellular fitness (28, 29). We did not observe
223 any significant difference in basal respiration between the untreated-NAC1 KO iTregs and WT
224 iTregs (**Figure 5B**); however, both the spare respiratory capacity (the ability of cells to respond
225 to changes in energetic demand) (**Figure 5C**) and maximal respiration (reflecting maximum
226 capacity of the electron respiratory chain) (**Figure 5D**) were significantly higher in NAC1 KO
227 iTregs than that in WT iTregs treated with LA or CM. These results imply that NAC1 KO Tregs
228 are more capable of meeting high energy demands in the acidic environment. Furthermore, we
229 examined the mitochondrial membrane potential of the Tregs using JC-1 staining. We observed
230 that the mitochondrial membrane potential of NAC1 KO iTregs was significantly higher than that
231 of WT iTregs in the presence of LA or CM (**Figure 5E-5H**). These results provide additional
232 evidence that NAC1-deficiency in Tregs appears to contribute to increased mitochondrial fitness
233 and biogenesis, enabling them to better meet the energy demands within the TME.

234

235 **Loss of NAC1 in Tregs facilitates their tumor infiltration and supports tumor progression**

236 Considering the crucial impact of NAC1 deletion on mitochondrial respiration (OXPHOS) and the
237 observed increases in OCR, FoxP3 expression, PGC1- α expression, lipid metabolism, and overall
238 metabolic fitness in NAC1-deficient Tregs in acidic conditions, we further validated our findings
239 by examining CD36 expression, lipid uptake, PGC-1 α expression, GzmB expression, and Treg
240 infiltration in B16-F10 tumors isolated from WT and NAC1KO mice. To assess lipid uptake and
241 CD36 expression, we first digested the tumor tissue using a tumor dissociation kit (Milteni Biotec),
242 isolated CD3 cells using a CD3 selection kit (BioLegend), and then stained these isolated CD3
243 cells with BODIPY 500/510 and CD36. lipid uptake (BODIPY 500/510) was significantly higher
244 in the intratumoral NAC1 KO Tregs than that in the intratumoral WT Tregs (**Figure 6A, 6B**).
245 Similarly, CD36 expression of the intratumor NAC1 KO Tregs was significantly higher than that
246 of WT Tregs (**Figure 6C, 6D**). Interestingly, both the intratumoral WT Tregs and NAC1 KO Tregs
247 had significantly higher CD36 expression than the splenic Tregs (**Figure 6C, 6D**). Moreover, the
248 infiltration of Tregs into the tumors was significantly higher in NAC1 KO mice (52.1%) than in
249 WT mice (31.4%) (**Figure 6E**). This observation was further confirmed by immune staining of
250 tumor tissue sections, which revealed a higher infiltration of CD36-expressing Tregs in NAC1 KO
251 mice (**Figure 1E**). Additionally, NAC1 KO intratumoral Tregs displayed higher expression of
252 FoxP3 (**Figure 6G, 6J**), GzmB (**Figure 6I, 6L**), and PGC-1 α (**Figure 6H, 6K**) compared to WT
253 intratumoral Tregs. These results confirmed that NAC1 deletion in Tregs lead to enhanced lipid
254 metabolism and mitochondrial biogenesis. Additionally, the enhanced infiltration and suppressive
255 effects of NAC1-deficient Tregs in the TME suggest that NAC1 deficiency in Tregs may
256 contribute to faster tumor initiation and growth in NAC1 KO mice compared to WT mice.

257

258 *Specific depletion of NAC1 in Tregs is a critical factor that supports tumor progression*

259 To further substantiates the role NAC1-deficient Tregs and its suppressive function of in tumor
260 progression, we conducted an adoptive transfer experiment in which the WT iTregs or NAC1
261 iTregs (Thy1.2⁺) were transferred into Thy1.1⁺ congenic recipient mice on day 1, and on the
262 following day, B16-F10 melanoma cells were *s.c.* injected into the flank of the recipient mice
263 (**Figure 7A**). Remarkably, the tumors in Thy1.1⁺ congenic recipient mice that received NAC1 KO
264 iTregs grew significantly faster than the tumors in mice that received WT iTregs (**Figure 7B**),
265 leading to shorter survival (**Figure 7C**). Similarly, MC38 tumors also exhibited significantly faster
266 growth in mice receiving NAC1 KO iTregs than tumors in mice receiving WT iTregs
267 (**Supplemental Figure 3A**). In another experiment, WT iTregs or NAC1 KO iTregs (Thy1.2⁺)
268 were adoptively transferred into Thy1.1⁺ congenic recipient mice following B16-F10 tumor
269 engraftment. The results demonstrated that NAC1 KO iTregs promoted tumor growth.
270 (**Supplemental Figure 7**). These experiments demonstrate that loss of NAC1 in Tregs causes their
271 metabolic reprogramming and enhances robustness of mitochondria in an acidic TME, leading to
272 increases of Treg infiltration. The enhanced PGC-1 α expression leads to increased lipid
273 metabolism, and mitochondrial fitness within the TME and contributing to tumor progression
274 (**Figure 7D**).

275 **Discussion**

276 NAC1 promotes glycolysis and the survival of hypoxic tumor cells, possibly through the direct
277 regulation of c-Myc. Deletion of NAC1 in tumor cells leads to oxidative stress, reduced LDHA
278 activity, and enhanced infiltration of cytotoxic T lymphocytes (CTLs) within the tumor mass (8).
279 Compared to Tconv, Tregs have a significantly reduced NAC1 expression. Deletion of NAC1
280 results in increased acetylation of FoxP3, leading to enhanced FoxP3 expression and the
281 suppressive function of Tregs. NAC1 deletion was found to impair T cell development in the
282 thymus. However, in peripheral blood and secondary lymphoid organs, Treg function is primarily
283 regulated by FoxP3, which is upregulated in the absence of NAC1. These findings suggest that
284 while NAC1 influences broader aspects of T cell biology, its effects on Tregs are largely FoxP3-
285 dependent (10). Additionally, the critical role of NAC1 in memory T cell development had been
286 also recently reported (4, 9). Prompted by our recent findings that NAC1 is a critical suppressor
287 of Treg development and function, and this role of NAC1 is mediated through epigenetic
288 regulation of FoxP3 expression and Treg stability (10), in the current study we investigated the
289 implications of the NAC1-mediated control of Tregs in tumor progression. We show here that
290 Tregs with deficiency in NAC1 have enhanced metabolic capacity to adapt to the acidic TME,
291 primarily through CD36/PGC-1 α -driven enhancement of mitochondrial fitness and lipid
292 metabolism, and NAC1-deficient Tregs promote tumor growth by increasing their tumor
293 infiltration and strengthening their suppressive function within the TME (**Figure 7D**).

294 Our analysis of Tregs from WT and NAC1 KO mice found that in the LA-containing media
295 or CM, the survival of NAC1 KO Tregs is prolonged as compared with that of WT Tregs (**Figure**
296 **2C, 2D**), suggesting that NAC1 deficiency confers a survival advantage to Tregs, allowing them
297 to thrive in the TME. This is likely due to the upregulation of FoxP3 expression in NAC1 KO
298 Tregs which reprograms T cell metabolism by suppressing glycolysis but promoting OXPHOS,

299 rendering Tregs resistant to lactate inhibition. The increased NAD:NADH ratio in Tregs, driven
300 by FoxP3-mediated metabolic changes, may enable them to effectively utilize lactate and convert
301 it into pyruvate and favor Tregs to survive in the TME where lactate is abundant. Indeed, we show
302 that lipid metabolism and mitochondria activity are enhanced in Tregs deficient in NAC1 when
303 cultured in the LA-rich media or CM (**Figure 3**). We also found that loss of NAC1 in Tregs results
304 in a significant increase in CD36 expression, a key fatty acid receptor, in Tregs cultured in CM
305 (**Supplemental Figure 2**) or on the tumoral Tregs (**Figure 6**). Selective upregulation of CD36 in
306 intratumoral Tregs and its role as a central metabolic modulator that finely tunes mitochondrial
307 fitness in the context of lactic acid-rich TME were reported previously (16, 21-23). This
308 upregulation was accompanied by an increased fatty acid uptake, as evidenced by BODIPY
309 500/510 staining (**Figure 4A**) and by an increase in neutral fat content, as indicated by BODIPY
310 493/503 staining, particularly in CN-treated or intratumoral NAC1 KO Tregs (**Figure 6A, 6B**).
311 Consistent with these findings, we also observed the upregulation of PGC-1 α , a critical regulator
312 of mitochondrial biogenesis in NAC1 KO Tregs. In Seahorse analysis, we found that NAC1 KO
313 Tregs display significantly higher levels of maximal respiration and spare respiratory capacity
314 cultured in CM (**Figure 5**). These observations imply that depletion of NAC1 leads to
315 upregulations of expressions of PGC-1 α , CD36, and fatty acid transport and metabolism,
316 collectively endowing NAC1 KO Tregs with increased metabolic vigor and adaptability within the
317 acidic TME.

318 Furthermore, NAC1 KO Tregs show a significant enhancement in their suppressive
319 function, as demonstrated by *in vitro* suppression assays (**Figure 3**) and evidenced by a substantial
320 increase in GzmB and TGF- β in NAC1 KO Tregs, particularly when cultured in CM (**Figure 3C,**
321 **3D**) or in the tumoral NAC1 KO Tregs (**Figure 3E, 3F**), implying that NAC1-deficient Tregs
322 possess higher suppressive activity over CTLs within the acidic TME. These results may explain

323 our *in vivo* experiments showing that absence of NAC1 in Tregs supports tumor growth in B16
324 melanoma (**Figure 7, Supplemental Figure 7**) and MC38 colon carcinoma models
325 (**Supplemental Figure 3A**). Additionally, IMC analysis of the tumor tissue sections shows that
326 the increased tumor infiltration of Tregs is associated with an increase in apoptotic CD8⁺ cells
327 expressing the PD1 marker (CD8⁺ PD1⁺) (**Figure 1F, 1G**). Together, these experiments pinpoint
328 the role of NAC1 in controlling the survival, metabolic fitness, and suppressive function of Tregs,
329 all are causally associated with immune evasion and the TME (14-17).

330 It is worth noting that the mice employed in this study were subjected to complete knockout
331 of the *NAC1* gene, therefore, the deficiency of NAC1 in other types of cells may also affect tumor
332 progression. In particular, the precise roles of NAC1 in other T cell subtypes, including CD8⁺ T
333 cells and conventional CD4⁺ T cells (e.g., Th1, Th2, Tfh, and Th17), and in innate immune cells
334 like macrophages and dendritic cells, are relatively unexplored. Thus, the exact impact of NAC1
335 on tumor development and progression remains to be further delineated.

336

337 **Materials and Methods**

338 *Sex as a biological variable*

339 Sex was not considered as a biological variable; both female and male mice were used.

340

341 *Cell lines and mice*

342 The B16-F10 (CRL-6475) melanoma cell line and MC38 CEA colon adenocarcinoma cell line
343 was cultured in Dulbecco's modified Eagle's medium (DMEM) with 10% fetal bovine serum
344 (FBS) and 1% penicillin-streptomycin and used for experiments when in the exponential growth
345 phase. All reagents were from Sigma-Aldrich (St Louis, MI). C57BL/6 (B6), Foxp3-IRES-mRFP
346 (FIR) reporter and Thy 1.1⁺ congenic mice were purchased from the Jackson Laboratory (Bar
347 Harbor, ME). NAC1 KO mice were generated by Dr. Jianlong Wang and crossed in the B6
348 background for more 10 generations (10). All the animal experiments were performed in
349 compliance with the regulations of The Texas A&M University Animal Care Committee (IACUC
350 no. 2018-0065) and in accordance with the guidelines of the Association for the Assessment and
351 Accreditation of Laboratory Animal Care.

352

353 *T cell culture and proliferation/cell division*

354 WT and NAC1 KO T cells isolated from mice using T cell isolation kits including mouse CD4⁺
355 (no. 130-104-454), CD8a⁺ (no. 130-104-075) and CD4⁺CD25⁺ Treg (no. 130-091-041) and were
356 activated by anti-mouse CD3 antibody (clone 2C11; BioLegend, San Diego, CA) plus anti-mouse
357 CD28 antibody (clone 37.51; BioLegend, San Diego, CA) in RPMI 1640 media with 10% FBS
358 (Omega Scientific, CA) and monitored for their survival by trypan blue cell exclusion method
359 using a TC20 automated cell counter (Bio-Rad, USA). *In vitro* T cell survival was determined

360 using trypan blue exclusion. Proliferation/division of T cells was measured using the CellTrace
361 CFSE Cell Proliferation Kit (no. C34554, Invitrogen).

362

363 *Cancer cell-conditioned medium and iTreg cell culture*

364 iTreg cells were generated by activating naïve CD4⁺ T cells with anti-CD3 (Clone#145-2C11) and
365 anti-CD28 (Clone #37.51) monoclonal antibodies (BioLegend) in RPMI 1640 media
366 supplemented with 10% FBS, 5 ng/ml transforming growth factor- β (TGF- β) and 5 ng/ml
367 interleukin-2 (r-IL-2) for 3 days. Then, activated CD4⁺ T cells were maintained in RPMI media
368 plus 10% FBS and 10 ng/ml for another 2 d. Differentiated iTreg cells were first sorted using a
369 fluorescence-activated cell sorting (FACS) cell sorter and then incubated in cancer cell-
370 conditioned medium and under the indicated culture conditions for 48 hours. Control RPMI 1640
371 for the treatment of iTreg cells in vitro was prepared with RPMI 1640 medium (Biological
372 Industries) supplemented with 2 mM glucose, 10 mM glutamine, 10% dialyzed FBS, 0.1% β -
373 mercaptoethanol and the indicated concentrations of lactic acids as we previously described (8).
374 B16-F10 cancer cell-conditioned medium was collected by incubating B16-F10 cells (70–80%
375 confluent) with the control RPMI 1640 described above for 18 hours. Then, the culture medium
376 was collected and centrifuged at 200 \times g. for 15 minutes to remove debris and cancer cells as
377 cancer cell-conditioned medium. B16-F10 cancer cell conditioned medium collected as described
378 above was passed through with 0.2 μ m membrane filter before Treg cell culture at a volume ratio
379 of 1:3.

380

381 *In vitro mouse Treg generation*

382 CD4⁺CD25⁻ naïve CD4 T cells sorted from spleen and LNs of WT or NAC1 KO or FIR mice from
383 CD4 cells enriched using a negative selection kit (MojoSort Mouse naïve CD4 T Cell Isolation

384 Kit; BioLegend). iTreg cells were generated by activating naive CD4⁺ T cells isolated from spleen
385 and LNs of WT or NAC1 KO mice with anti-CD3 plus anti-CD28 monoclonal antibodies
386 (BioLegend) in RPMI 1640 media supplemented with 10% FBS, 5 ng/ml TGF- β and 5 ng/ml rIL-
387 2 for 3 days. Then, activated CD4⁺ T cells were maintained in RPMI 1640 media plus 10% FBS
388 and 10 ng/ml for another 48 hours. Efficiency of iTreg differentiation was determined by FACS
389 analysis.

390

391 *Flow cytometry, cell sorting and antibodies*

392 Single-cell suspensions were incubated with TruStain FcX™ (anti-mouse CD16/32) antibodies
393 (BioLegend) on ice for 10 minutes before staining. Cell suspensions were first stained using a
394 LIVE/DEAD Fixable Violet Dead Cell Stain Kit (Thermo Fisher Scientific) or Zombie NIR™
395 Fixable Viability Kit (BioLegend) or Zombie Aqua™ Fixable Viability Kit (BioLegend) at 37 °C
396 for 10 min. After washing, surface markers were stained for 30 minutes at 4 °C. Intracellular
397 staining was performed after incubation of single-cell suspensions with BD GolgiStop from BD
398 Biosciences (#AB_2869012, San Diego, CA, USA) in medium for 4 hours using Intracellular
399 Staining Permeabilization Wash Buffer and Fixation Buffer from BioLegend (#421002, San
400 Diego, CA, USA). Apoptosis was determined by staining with Apotracker™ Green (#427402).
401 Samples were analyzed on BD Fortessa X-20 flow cytometers (BD Biosciences) and data were
402 analyzed with FlowJo as gating strategy shown in **Supplemental Figure 6**. Cells were sorted on
403 FACS Aria III sorter (BD Biosciences). Tregs were defined by the following staining:
404 Live/Dead–CD45–CD3⁺CD4⁺CD8⁻CD25⁺ FoxP3⁺. CD8 T cells were defined by the following
405 staining: CD45⁺CD3⁺CD8⁺CD4⁻. The following antibodies against mouse proteins were used:
406 anti-CD45 (Clone #30-F11), anti-CD3 ϵ (Clone #17A2), anti-CD4 (Clone #RM4-5), anti-CD8 α
407 (Clone #53.6.7), anti-CD44 (Clone #IM7), anti-CD4 (Clone #GK1.5), anti-CD8 (Clone #53-6.7),

408 anti-CD25 (Clone #3C7), anti-CD36 (Clone #HM36), anti-FoxP3 (Clone #MF-14), anti-GFP/YFP
409 (Clone #FM264G), Thy1.2 (Clone #140331), anti-PGC-1 α , and anti-a. These antibodies were
410 purchased from BioLegend, Thermo Scientific, eBiosciences or Cell Signaling.

411

412 *Tumor engraftment and Murine melanoma models*

413 Before tumor induction, 8–10-week-old mice were shaved on back on the skin surface, to induce
414 tumor formation. For tumor engraftment, 3×10^6 cells B16-F10 or 3×10^6 MC38 tumor cells in 100
415 μ l phosphate-buffered saline were injected subcutaneously into the right flank of B6. Thy1.1 or
416 WT or NAC1KO mice. Tumors were measured every 2–3 days after tumor engraftment and
417 calculated. Tumor volumes were calculated by volume = (length \times width²)/2 for engrafted tumors
418 or volume = (length \times width \times height) for inducible tumors. When mice-bearing tumors reach a
419 maximum size of 2,000 mm³, tumors were prepared for analysis. All experiments were conducted
420 according to Swiss federal regulations.

421

422 *Tumor digestion and cell isolation*

423 Tumors were washed with PBS and minced into small pieces in RPMI containing the enzyme mix
424 of mouse tumor dissociation kit (Miltenyi Biotec; #130-096-730). Tumor digestion was done
425 according to the manufacturer protocol. Single cell suspension was filtered through a 100 μ m cell
426 strainer and washed with PBS. Tumor cells were incubated with RBC Lysing Buffer (BD) to lyse
427 red blood cells and then washed with FACS buffer (phosphate-buffered saline with 2% FBS and
428 2 mM EDTA). Tumor-infiltrating T cells were further enriched by CD3 cells selection kit
429 (BioLegend) as described by manufacturer. Cells were further stained and analyzed by FACS
430 analysis.

431

432 *Imaging mass cytometry (IMC) analysis*

433 IMC uses heavy metal label-conjugated antibodies, greatly enhancing the deep
434 immunophenotyping analysis of tumor samples. A dimensionality reduction technique, *t*-SNE,
435 was used to analyze several tumor-associated immune cell markers in the WT vs. NAC1 KO
436 groups of mice. A bar graph of the number of cells per neighborhood across the imaged tumor
437 samples were constructed to analyze the local cell densities within individual neighborhoods as
438 described previously (30). Ir191, Er167, Dy162, Er170Sm149, and Yb176 were used for staining
439 DNA, Ki-67 Ag, CD8⁺ T cells, B220 (B cells), CD11b (dendritic cells), and F4/80 (macrophages),
440 respectively.

441

442 *Mitochondrion, fatty acid uptake and lipid content assay*

443 To measure mitochondrial membrane potential, cells were washed and incubated with prewarmed
444 (37 °C) staining solution (DPBS with 1% FBS) and stained with JC-1 assay kit (M34152; Thermo
445 Scientific) at working concentrations of 1 μM for 30 minutes as suggested by manufacturer. After
446 staining, the cells were washed and resuspended in fresh FACS buffer for surface marker staining,
447 as described above. To measure fatty acid uptake, cells were incubated in RPMI 1640 medium (or
448 human T cell culture medium) containing C1-BODIPY 500/510 C12 (Life Technologies) at a final
449 concentration of 0.5 μM for 15 minutes at 37°C. After incubation, cells were washed with FACS
450 buffer for surface staining. For lipid content detection, after permeabilization and fixation, cells
451 were stained using BODIPY 493/503 (Life Technologies) at a final concentration of 500 ng/ml
452 together with other intracellular markers.

453

454 *Adoptive T cell transfer*

455 Naive CD4⁺ T cells were harvested using a combination of negative magnetic selection (MojoSort
456 Mouse CD4 T Cell Isolation Kit; BioLegend) and FACS sorting (>98% purity) from spleen and
457 LNs of WT or NAC1 KO mice and cultured in polarizing condition to Treg as mentioned above.
458 On day 0, approximately 3 x 10⁶ WT and NAC1 KO iTreg (day 5) were *i.p.* injected into two
459 separate groups of Thy1.1 mice (n=5) prepared for tumor engraftment. On day 1, 3 x 10⁶ B16-F10
460 melanoma or MC32 CEA tumor were *s.c.* injected into each of the recipient mice of both groups
461 and tumor progression were monitored. The mice were monitored for survival and tumor size up
462 to day 28 after tumor induction. The experiment was terminated on day 28, and the explanted
463 tumor was analyzed by flow cytometry, image mass cytometry, and confocal microscopy as
464 described (30).

465

466 *Tumor imaging and immunohistochemistry*

467 Tumor tissues were fixed with 10% neutral formalin solution (VWR, West Chester, PA, USA) for
468 24 hours. and placed in the labeled cassettes for further embedding in molten paraffin wax. From
469 the fixed samples in paraffin block tissue sections at a thickness of 3–5 μm were prepared and
470 stained with H&E as described. For immunofluorescence microscopy, the tissues were frozen in
471 cryovials on dry ice immediately following resection. Cryo-sectioning and immunofluorescence
472 staining were performed as described (30). Alexa Fluor 488-CD36 (Abcam), Alexa Fluor 647-
473 FoxP3 (BioLegend) and eFluor 570-Thy1.1 (Thermo) from BioLegend (San Diego, CA) were used
474 to detect the tumor-infiltrating Tregs.

475

476 *Ex vivo Treg suppression assay*

477 CD8⁺ T cells from the spleens and LNs of Thy1.1 mice were enriched using a negative selection
478 kit (MojoSort Mouse CD8 T Cell Isolation Kit; BioLegend) and stained with a CellTrace CFSE

479 Cell Proliferation Kit (Thermo Fisher Scientific) for 10 minutes at RT. A total of 2.5×10^4 CD8⁺
480 cells were seeded into a CD3 (4 µg/ml) coated 96-well round plate in RPMI 1640 medium
481 containing of 4 µg/ml CD28. CD4⁺CD25⁺ Tregs sorted from spleen and LNs of WT and NAC1
482 KO mice. CD4 T cells enriched using a negative selection kit (MojoSort Mouse CD4 T Cell
483 Isolation Kit; BioLegend) were added according to the indicated ratios for Treg to effector T cell
484 (Teff). Then 5 ng/ml rIL2 were supplemented into cultures media. As negative controls,
485 CD4⁺CD25⁺ Tregs and CD4⁺CD25⁻ responder T cells were cultured without any stimulus. Cells
486 were incubated at 37 °C under 5% CO₂ for 72 hours and then the proliferation of CD8⁺ T cells
487 was determined by CFSE dilution with flow cytometry analysis and Suppression of responder T
488 cells was determined.

489

490 *Metabolic profiling: Seahorse Assay*

491 Seahorse XF Cell mito stress test was performed with a Seahorse XF96 Extracellular Flux
492 Analyzer using Seahorse XF Cell mito stress test kit (#103010-100; Agilent) according to the user
493 guides provided with kit. Approximately 2×10^5 cells iTregs were plated in the Cell-Tak-coated
494 Seahorse Bioanalyzer XFe96 culture plates in assay medium consisting of minimal RPMI 1640
495 medium supplemented with 1% bovine serum albumin (BSA) and 25 mM glucose, 2 mM
496 glutamine and 1 mM sodium pyruvate. Basal rates were taken for 30 min and a set of drugs,
497 oligomycin (2 mM), FCCP (0.5 mM), and rotenone/antimycin A (0.5 mM) were injected into each
498 sample at different times and readings were measured at every 3 minutes for 1 to 2 hours. Each
499 condition was analyzed, with 6-12 replicates in each single experiment. The Extra Cellular
500 Acidification Rate (ECAR) was measured in the glycolytic rate and the Oxygen Consumption Rate
501 (OCR) was tested to indicate oxidative phosphorylation.

502

503 *TCGA bioinformatics analysis*

504

505 The bioinformatic analysis was conducted using data collected from The Cancer Genome Atlas
506 (TCGA) database, accessed through the GEPIA2 web server (<http://gepia2.cancer-pku.cn/>). Two
507 specific TCGA subtypes were analyzed: Kidney Renal Clear Cell Carcinoma (KIRC) and
508 Glioblastoma Multiforme (GBM). The focus of the analysis was on the expression of regulatory T
509 cells (Tregs), annotated by the markers FOXP3, CTLA4, CCR8, and TNFRSF9. These curves
510 were generated to compare high versus low expression groups for each marker, providing insights
511 into the prognostic significance of Treg expression in KIRC and GBM. The overall survival (OS)
512 and disease-free survival (DFS) rates associated with the expression levels of these Treg markers
513 were illustrated using Kaplan-Meier survival curves. Statistical analyses were performed to assess
514 the significance of survival differences between the high and low expression groups. The log-rank
515 test was employed to determine the p-values, and a p-value of less than 0.05 was considered
516 statistically significant.

517

518 *Statistical analysis*

519 Paired or unpaired Student's t-test or one-way or two-way ANOVA was performed to analyze the
520 differences between the groups, using GraphPad Prism (GraphPad Software, San Diego, CA). For
521 mice survival curve analysis, the Kaplan-Meier method was adopted and compared statistically
522 using the log-rank test in GraphPad Prism. Each point represented a biological replicate, and all
523 data are presented as means \pm s.d. or means \pm s.e.m., as indicated. *P* values ($***P < 0.001$, $**P <$
524 0.01 and $*P < 0.05$) are labeled in the figures. $P < 0.05$ was considered statistically significant.
525 The illustrations and schematic representations in figures are created by using the BioRender
526 software.

527

528 *Data availability*

529 The datasets shown in all the figures are listed in an associated spreadsheet of Supporting Data

530 Values.

531

532 **Data availability statement:** All data supporting the findings of this study are available in the main
533 text and its supplementary information. Further information is available from the corresponding
534 authors on reasonable request.

535

536 **Author Contributions:** A.K. and J.S. conceptualized the research project, A.K. designed and
537 performed the experiment, analyzed the data, and wrote the manuscript. X.X. did breeding
538 maintenance of animals used in this study and monitored mice. J.K.D., H.-Y.P., L.W., D.J.B., and
539 Y.R., assisted in data analysis and revised the manuscript. J.-M.Y., and P.d.F., reviewed, advised,
540 and revised the manuscript. J.-M.Y., P.d.F., and J.S. supervised the overall project and reviewed,
541 advised, and revised the manuscript. J.-M.Y. and J.S. are the guarantors for the overall content of
542 this work. All authors read and approved the final version of the manuscript. Guarantor's
543 statement: J.-M.Y. and J.S. are the guarantors of this work and, as such, had full access to all the
544 data in the study and takes responsibility for the integrity of the data and the accuracy of the data
545 analysis.

546

547 **Acknowledgments:** We thank Dr. Jianlong Wang at Columbia University Irving Medical Center
548 for providing NAC1 KO mice. We thank S.-H. Chen at the Houston Methodist Research Institute
549 for the IMC analysis. We acknowledge Ms. Robbie Moore from The School of Medicine Cell
550 Analysis Facility (SOM-CAF) at the Texas A&M Health Science Center for cell sorting. We thank
551 Dr. Malea Muriel Murphy from Integrated Microscope and Imaging Laboratory at Texas A&M
552 Health Science Center for imaging analysis.

553

554 **Funding:** This work was supported by National Institutes of Health Grant R01CA221867 and
555 R21AI167793 to J.S., R01CA273002 to J-M. Y and J. S., and Department of Defense Grant
556 LC210150 to J. S.

557

558 **Conflicts of interest:** P.d.F. and J.S. have affiliation with Tranquility Biodesign, LLC, which has
559 intellectual property unrelated to this manuscript. J.S. is an inventor on a pending patent (U.S.
560 Application No.: 63/291,462) related to this work filed by Texas A&M University (TAMUS 5869,
561 filed on 20 December 2022). The authors declare no other competing interests.

562

563 **References:**

564

- 565 1. Rahman MT, Nakayama K, Ishikawa M, Rahman M, Katagiri H, Katagiri A, et al. NAC1,
566 a BTB/POZ protein overexpressed in uterine sarcomas. *Anticancer Res.* 2012;32(9):3841-
567 5.
- 568 2. Chen F, Yin Y, Yan Z, Cao K, and Zhong K. NAC1 promotes the migration of prostate
569 cancer cells and participates in osteoclastogenesis by negatively regulating IFNbeta. *Oncol*
570 *Lett.* 2018;15(3):2921-8.
- 571 3. Wang X, Ji C, Zhang H, Shan Y, Ren Y, Hu Y, et al. Identification of a small-molecule
572 compound that inhibits homodimerization of oncogenic NAC1 protein and sensitizes
573 cancer cells to anticancer agents. *J Biol Chem.* 2019;294(25):10006-17.
- 574 4. Wang L, Peng HY, Kishore Das J, Kumar A, Ren Y, Ballard DJ, et al. NAC1 confines
575 virus-specific memory formation of CD4(+) T cells through the ROCK1-mediated pathway.
576 *J Med Virol.* 2023;95(7):e28957.
- 577 5. Wang L, Das JK, Kumar A, Peng HY, Ren Y, Xiong X, et al. Autophagy in T-cell
578 differentiation, survival and memory. *Immunol Cell Biol.* 2021;99(4):351-60.
- 579 6. Ueda SM, Yap KL, Davidson B, Tian Y, Murthy V, Wang TL, et al. Expression of Fatty
580 Acid Synthase Depends on NAC1 and Is Associated with Recurrent Ovarian Serous
581 Carcinomas. *J Oncol.* 2010;2010:285191.
- 582 7. Zhang Y, Ren YJ, Guo LC, Ji C, Hu J, Zhang HH, et al. Nucleus accumbens-associated
583 protein-1 promotes glycolysis and survival of hypoxic tumor cells via the HDAC4-HIF-
584 1alpha axis. *Oncogene.* 2017;36(29):4171-81.
- 585 8. Ren Y, Kumar A, Das JK, Peng H-Y, Wang L, Ballard D, et al. Tumorous expression of
586 NAC1 restrains antitumor immunity through the LDHA-mediated immune evasion.
587 *Journal for immunotherapy of cancer.* 2022;10(9):e004856.
- 588 9. Wang L, Kumar A, Das JK, Ren Y, Peng H-Y, Ballard DJ, et al. Expression of NAC1
589 Restrains the Memory Formation of CD8+ T Cells during Viral Infection. *Viruses.*
590 2022;14(8):1713.
- 591 10. Yang J-M, Ren Y, Kumar A, Xiong X, Das JK, Peng H-Y, et al. NAC1 modulates
592 autoimmunity by suppressing regulatory T cell-mediated tolerance. *Science Advances.*
593 2022;8(26):eabo0183.
- 594 11. Chou WC, Guo Z, Guo H, Chen L, Zhang G, Liang K, et al. Author Correction: AIM2 in
595 regulatory T cells restrains autoimmune diseases. *Nature.* 2021;592(7856):E29.
- 596 12. Saleh R, and Elkord E. FoxP3(+) T regulatory cells in cancer: Prognostic biomarkers and
597 therapeutic targets. *Cancer Lett.* 2020;490:174-85.
- 598 13. Gong Z, Jia H, Yu J, Liu Y, Ren J, Yang S, et al. Nuclear FOXP3 inhibits tumor growth
599 and induced apoptosis in hepatocellular carcinoma by targeting c-Myc. *Oncogenesis.*
600 2020;9(10):97.
- 601 14. Angelin A, Gil-de-Gomez L, Dahiya S, Jiao J, Guo L, Levine MH, et al. Foxp3 Reprograms
602 T Cell Metabolism to Function in Low-Glucose, High-Lactate Environments. *Cell Metab.*
603 2017;25(6):1282-93 e7.
- 604 15. Watson MJ, Vignali PDA, Mullett SJ, Overacre-Delgoffe AE, Peralta RM, Grebinoski S,
605 et al. Metabolic support of tumour-infiltrating regulatory T cells by lactic acid. *Nature.*
606 2021;591(7851):645-51.
- 607 16. Wang H, Franco F, Tsui YC, Xie X, Trefny MP, Zappasodi R, et al. CD36-mediated
608 metabolic adaptation supports regulatory T cell survival and function in tumors. *Nat*
609 *Immunol.* 2020;21(3):298-308.

- 610 17. Luengo A, Li Z, Gui DY, Sullivan LB, Zagorulya M, Do BT, et al. Increased demand for
611 NAD(+) relative to ATP drives aerobic glycolysis. *Mol Cell*. 2021;81(4):691-707 e6.
- 612 18. Cao X, Cai SF, Fehniger TA, Song J, Collins LI, Piwnica-Worms DR, and Ley TJ.
613 Granzyme B and perforin are important for regulatory T cell-mediated suppression of
614 tumor clearance. *Immunity*. 2007;27(4):635-46.
- 615 19. Tibbs E, Kandy R, Jiao D, Wu L, and Cao X. Murine regulatory T cells utilize granzyme
616 B to promote tumor metastasis. *Cancer Immunol Immunother*. 2023.
- 617 20. Sun B, Liu M, Cui M, and Li T. Granzyme B-expressing treg cells are enriched in colorectal
618 cancer and present the potential to eliminate autologous T conventional cells. *Immunol Lett*.
619 2020;217:7-14.
- 620 21. Chen Y, Zhang J, Cui W, and Silverstein RL. CD36, a signaling receptor and fatty acid
621 transporter that regulates immune cell metabolism and fate. *J Exp Med*. 2022;219(6).
- 622 22. Liao X, Yan S, Li J, Jiang C, Huang S, Liu S, et al. CD36 and Its Role in Regulating the
623 Tumor Microenvironment. *Curr Oncol*. 2022;29(11):8133-45.
- 624 23. Tao L, Ding X, Yan L, Xu G, Zhang P, Ji A, and Zhang L. CD36 accelerates the
625 progression of hepatocellular carcinoma by promoting FAs absorption. *Med Oncol*.
626 2022;39(12):202.
- 627 24. Rahman MT, Nakayama K, Rahman M, Katagiri H, Katagiri A, Ishibashi T, et al. Fatty
628 acid synthase expression associated with NAC1 is a potential therapeutic target in ovarian
629 clear cell carcinomas. *Br J Cancer*. 2012;107(2):300-7.
- 630 25. Xu S, Chaudhary O, Rodriguez-Morales P, Sun X, Chen D, Zappasodi R, et al. Uptake of
631 oxidized lipids by the scavenger receptor CD36 promotes lipid peroxidation and
632 dysfunction in CD8(+) T cells in tumors. *Immunity*. 2021;54(7):1561-77 e7.
- 633 26. Supruniuk E, Miklosz A, and Chabowski A. The Implication of PGC-1alpha on Fatty Acid
634 Transport across Plasma and Mitochondrial Membranes in the Insulin Sensitive Tissues.
635 *Front Physiol*. 2017;8:923.
- 636 27. LeBleu VS, O'Connell JT, Gonzalez Herrera KN, Wikman H, Pantel K, Haigis MC, et al.
637 PGC-1alpha mediates mitochondrial biogenesis and oxidative phosphorylation in cancer
638 cells to promote metastasis. *Nat Cell Biol*. 2014;16(10):992-1003, 1-15.
- 639 28. Marchetti P, Fovez Q, Germain N, Khamari R, and Kluza J. Mitochondrial spare
640 respiratory capacity: Mechanisms, regulation, and significance in non-transformed and
641 cancer cells. *FASEB J*. 2020;34(10):13106-24.
- 642 29. Gu X, Ma Y, Liu Y, and Wan Q. Measurement of mitochondrial respiration in adherent
643 cells by Seahorse XF96 Cell Mito Stress Test. *STAR Protoc*. 2021;2(1):100245.
- 644 30. Das JK, Ren Y, Kumar A, Peng HY, Wang L, Xiong X, et al. Elongation factor-2 kinase
645 is a critical determinant of the fate and antitumor immunity of CD8(+) T cells. *Sci Adv*.
646 2022;8(5):eabl9783.

647

648 **Figure Legends**

649 **Figure 1. NAC1 deficiency supports tumor growth in mice.** B16F10 melanoma cells (3×10^6
650 cells/mouse) were *s.c.* inoculated into WT and NAC1 KO mice and the tumors were harvested for
651 histology examination. (A) Tumor growth curves (n=5). (B) Representative survival curve was
652 plotted. (C-E) Tumors were harvested and examined for the infiltration of lymphocytes by H&E
653 staining (D) and) FoxP3-expressing Tregs by IHC staining (E). (F) *t*-SNE plot showing
654 quantification of infiltrating immune cells population in WT vs. NAC1 KO generated by IMC
655 analysis was performed with the tumor tissue section. (G) Quantification of infiltrating immune
656 cell population analyzed by IMC analysis.

657

658 **Figure 2. NAC1 KO Tregs show prolonged survival and enhanced polarization in acidic**
659 **environments.** (A) Representative flow cytometry shows FoxP3⁺CD25⁺ Treg frequency
660 following LA and CM treatment. (B) Proliferation of Tregs as determined by CFSE staining (n=3).
661 (C) Representative plots of Apotracker green and Live-Dead expression on the WT and NAC1
662 KO Tregs treated with LA or CM for 48 hours (n=3).

663

664 **Figure 3. NAC1 KO Tregs show enhanced functional activity of Tregs in acidic**
665 **environments.** (A) CD8 cells were labelled with CFSE and co-cultured with WT or NAC1 KO
666 Tregs (1:1) in the presence of anti-CD3 and CD28 antibodies. Histogram of representative
667 experiment showing the proliferation CD8 cells in the CM-treated culture. (B) Quantification
668 analysis of the in vitro suppression assay (n=3). (C) Representative histogram of the expression of
669 GrazB in WT and NAC1 KO Tregs after 48-hour treatment with LA or CM (n=5). (D)
670 Quantification of differential expression of GrazB in WT vs. NAC1 KO Tregs after the indicated
671 treatment for 48 hours (n=5). (E) Representative histogram of TGF- β expression in WT Tregs and

672 NAC1 KO Tregs after 48-hour treatment with LA or CM (n=5). (F) Quantification of differential
673 expression of TGF- β in WT Tregs vs. NAC1 KO Tregs after the indicated treatment for 48 hours
674 (n=5).

675

676 **Figure 4. NAC1 KO Tregs have elevated lipid uptake and neutral lipid content in an acidic**
677 **condition.** (A) Representative histogram of lipid content measured by BODIPY 493/503 staining
678 in Tregs in the indicated culture conditions. (B) Representative histogram of fatty acid uptake
679 measured by C1-BODIPY 500/510 C12 staining in Tregs in the indicated culture conditions. (C)
680 Quantification of fatty acid uptake (C1-BODIPY 500/510 C12; n=5). (D) Quantification of lipid
681 content (BODIPY 493/503; n=5). (E) Representative histogram of PGC-1 α expression in WT and
682 NAC1 KO Tregs in the indicated culture conditions. (F) Quantification of PGC-1 α expression in
683 WT and NAC1 KO Tregs in the indicated culture conditions. The differences were analyzed by
684 Two-way ANOVA with multiple comparisons correction using GraphPad prism software. ***:
685 $p \leq 0.001$.

686

687 **Figure 5. NAC1 KO Tregs show enhanced mitochondrial respiration in an acidic**
688 **environment.** (A) Effect of LA or CM treatment on mitochondrial respiration of WT and NAC1
689 KO Tregs, as measured by Seahorse XFe96 Metabolic Analyzer. Data are represented as mean \pm
690 SEM; n=6 per condition from two independent experiments. (B) Basal respiration. (C) Spare
691 respiratory capacity. (D) Maximum respiration quantified by seahorse wave 3.0 software. The
692 differences were analyzed by Two-way ANOVA with multiple comparisons correction using
693 GraphPad prism software. ***: $p \leq 0.001$. (E – H) The mitochondrial membrane potential of WT
694 vs. NAC1 KO Tregs measured by JC-1 staining. (E) Untreated. (F) 10mM LA. (G) CM. (H)
695 Quantification of mitochondrial membrane potential (n=5. The differences were analyzed by Two-

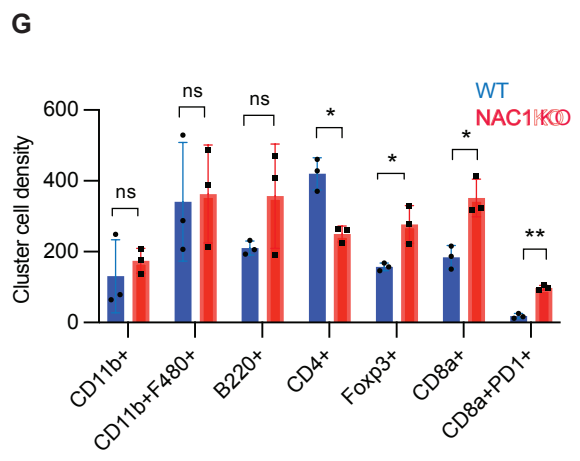
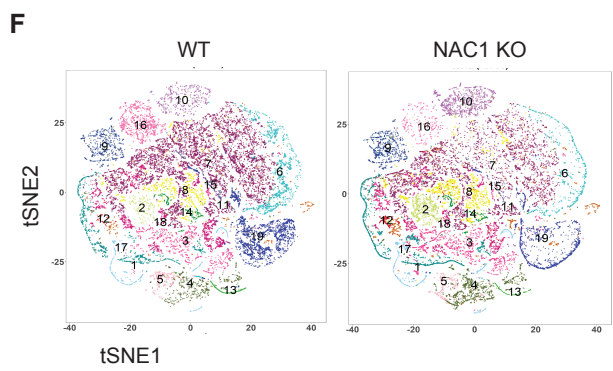
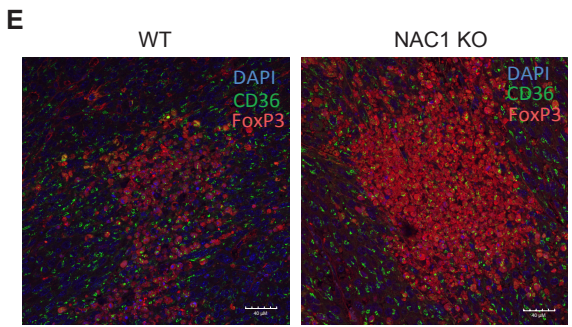
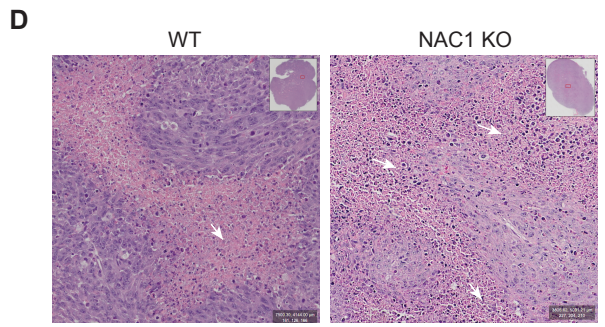
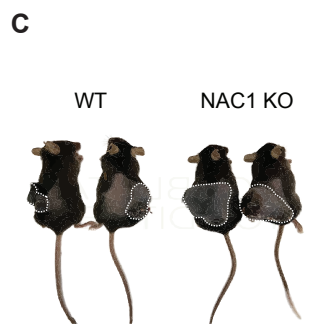
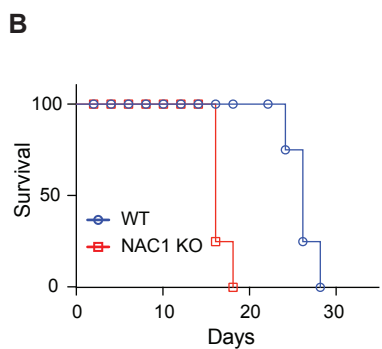
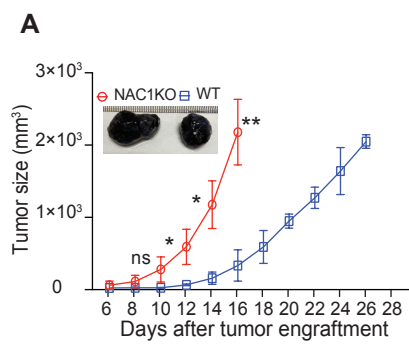
696 way ANOVA with multiple comparisons correction using GraphPad prism software. ***:
697 $p \leq 0.001$.

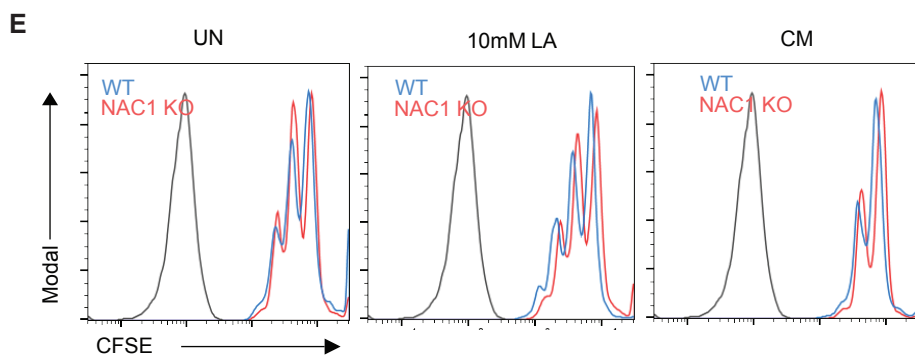
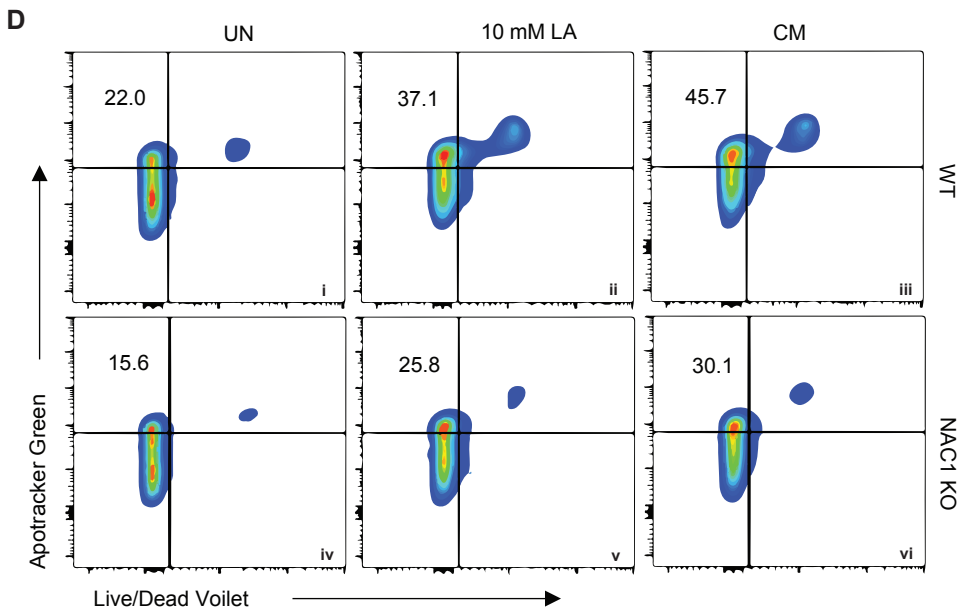
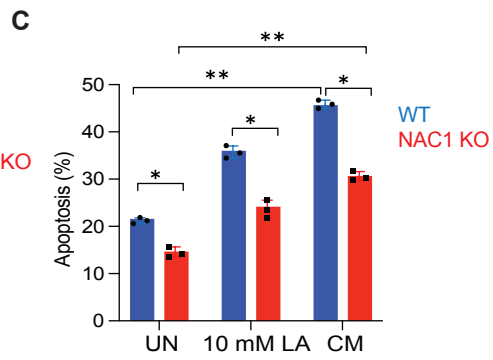
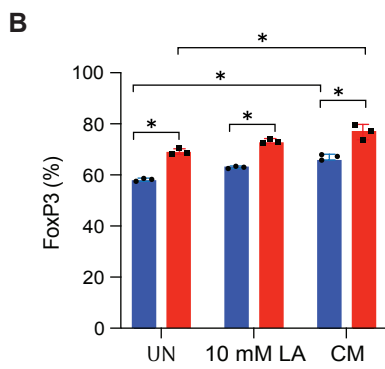
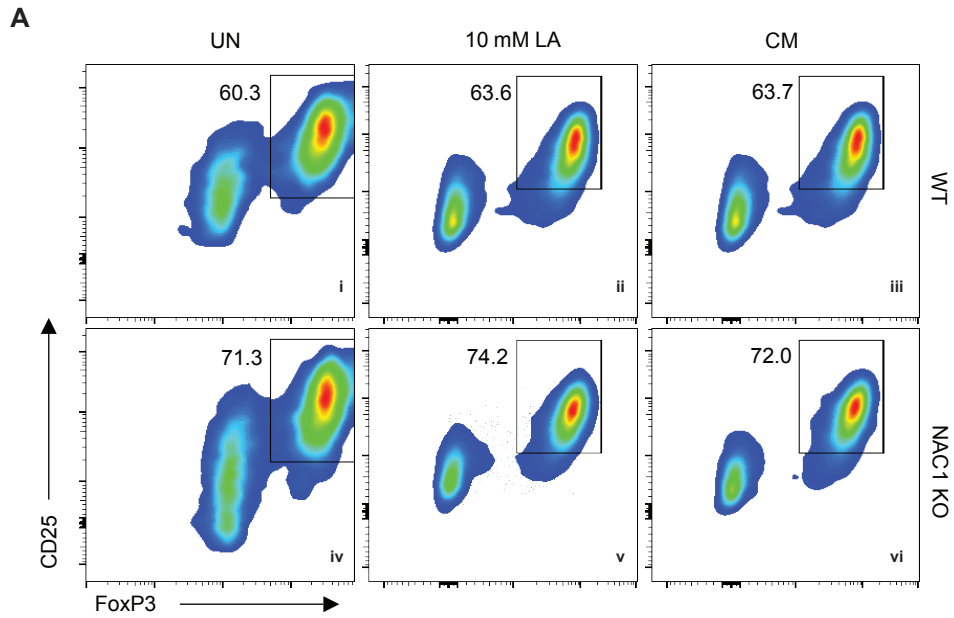
698

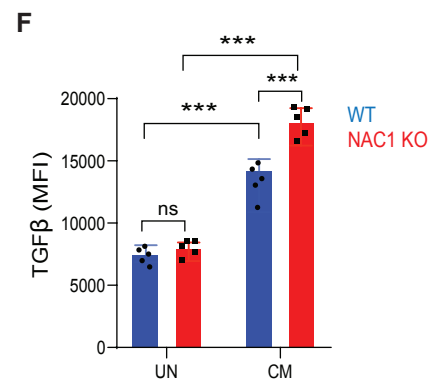
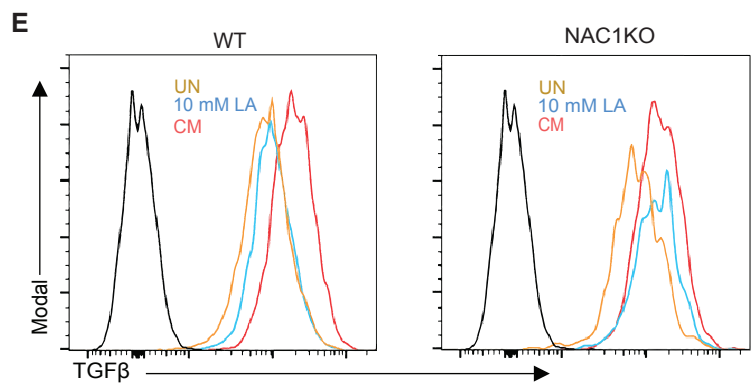
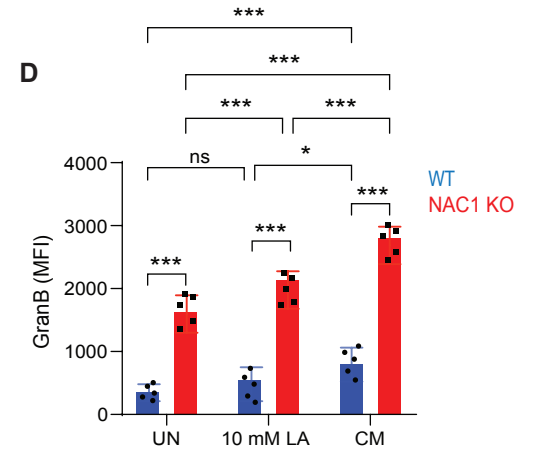
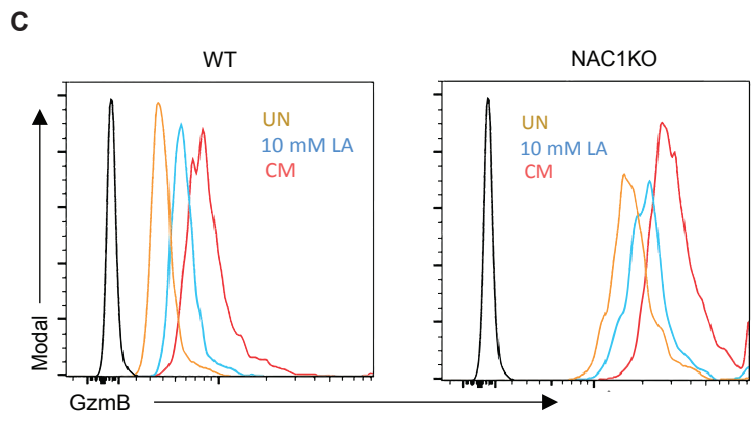
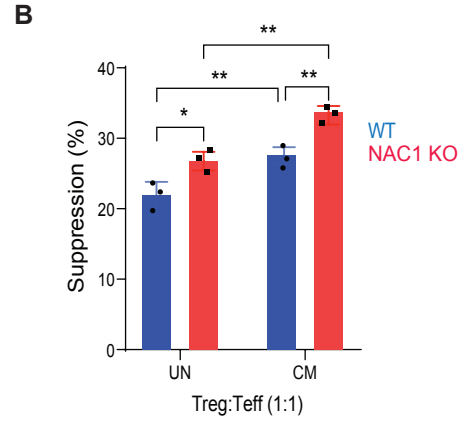
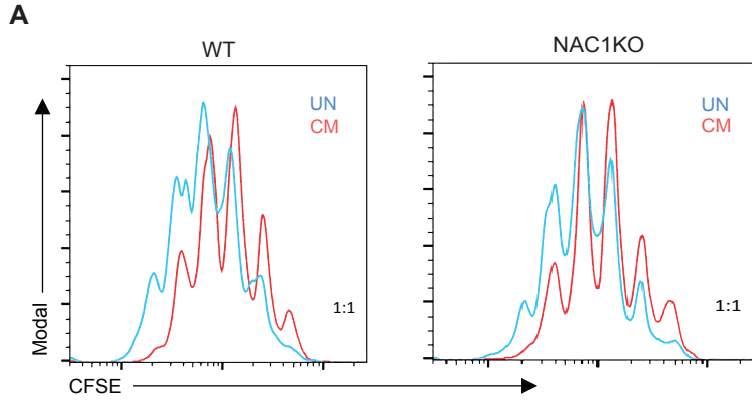
699 **Figure 6. NAC1 KO Tregs are robust in the TME.** B16F10 tumors from WT or NAC1 KO mice
700 were harvested, dissociated, and the tumoral Tregs were stained and analyzed by Flow cytometry.
701 **(A, B)** Fatty acid uptake of intratumoral Tregs and splenic Tregs as measured by C1-BODIPY
702 500/510 C12. **(A)** Representative histogram; **(B)** Quantification of fatty acid uptake. **(C, D)** CD36
703 expression in intratumoral Tregs and splenic Tregs. **(C)** Representative histogram; **(D)**
704 Quantification of CD36 expression (n=3). The differences were analyzed by Two-way ANOVA
705 with multiple comparisons correction using GraphPad prism software. ***: $p \leq 0.001$. **(E)**
706 FoxP3⁺CD4⁺ Treg frequency in tumors isolated from WT or NAC1KO mice. Representative
707 histogram of expression of FoxP3 **(F)**, PGC-1 α **(G)** and GrazB **(H)**, and their quantification:
708 FoxP3 **(I)**, PGC-1 α **(J)**, and GrazB **(K)**. (n=4). The differences were analyzed by Two-way
709 ANOVA with multiple comparisons correction using GraphPad prism software. ***: $p \leq 0.001$.

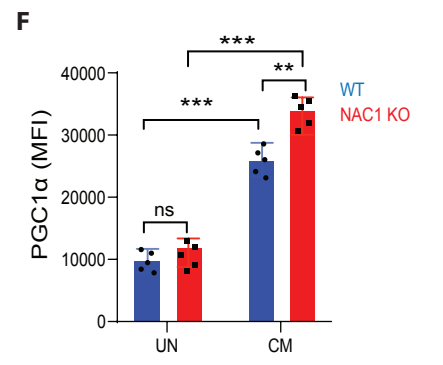
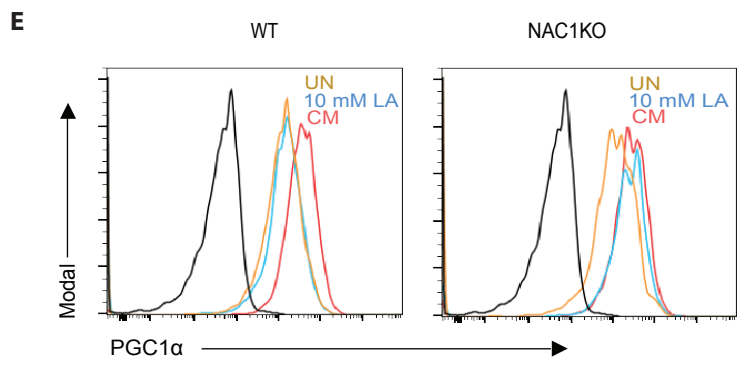
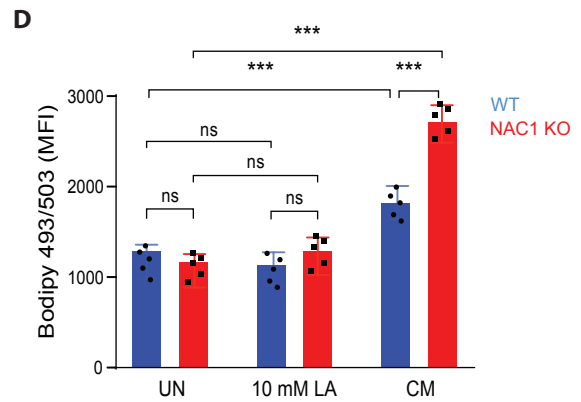
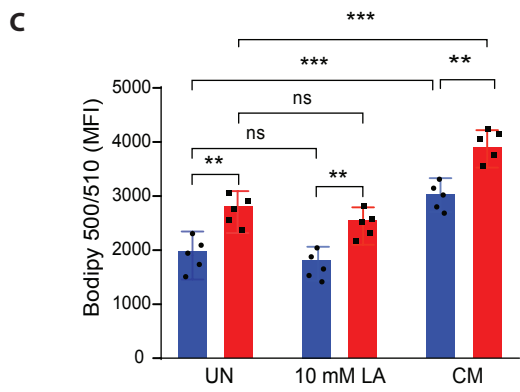
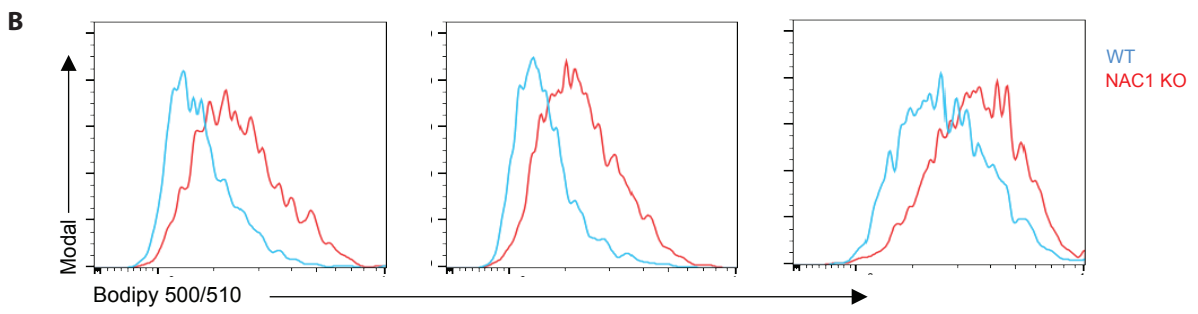
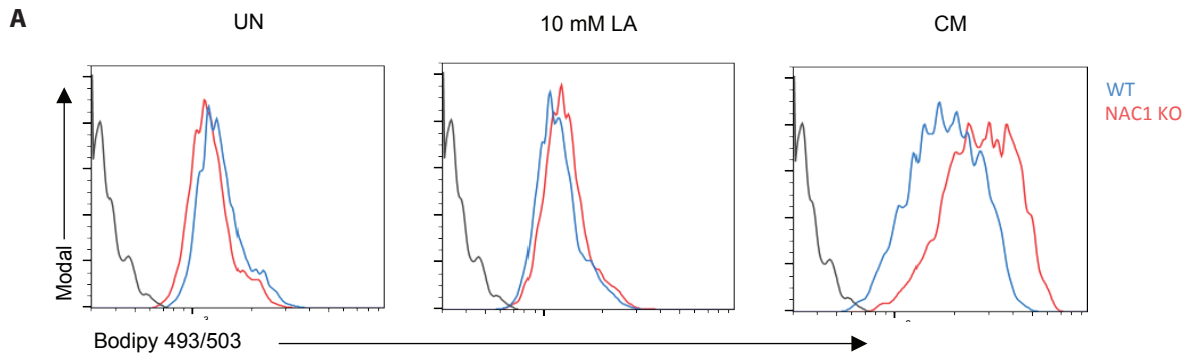
710

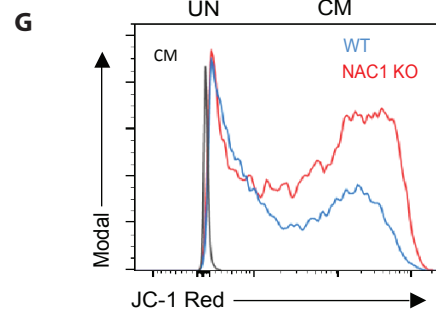
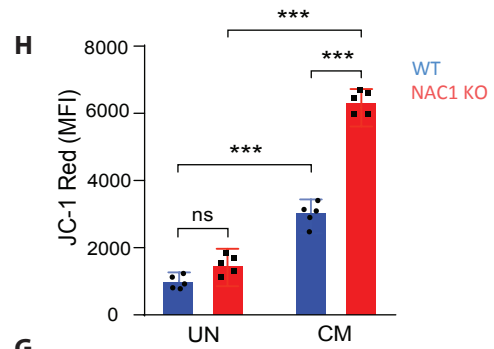
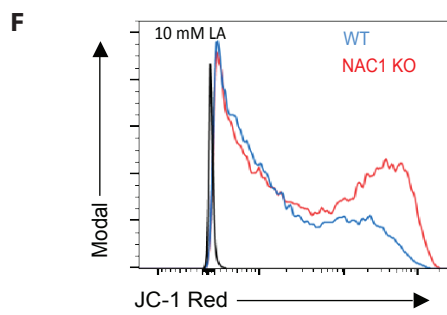
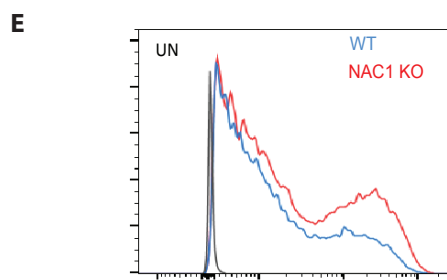
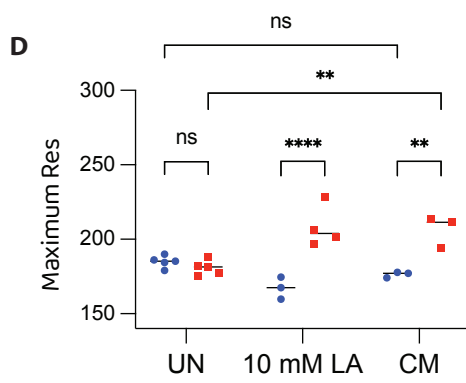
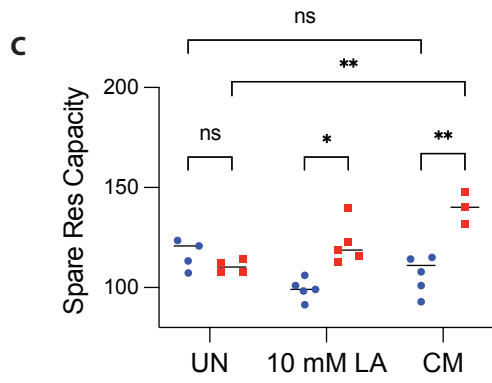
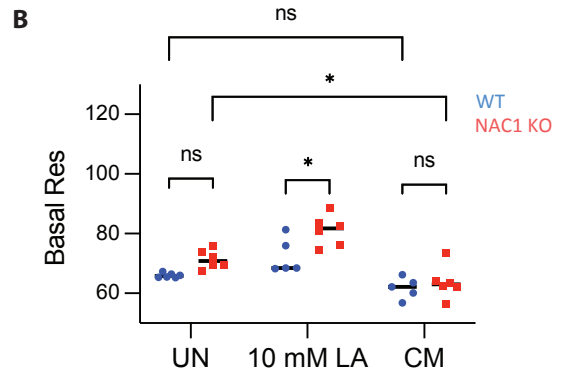
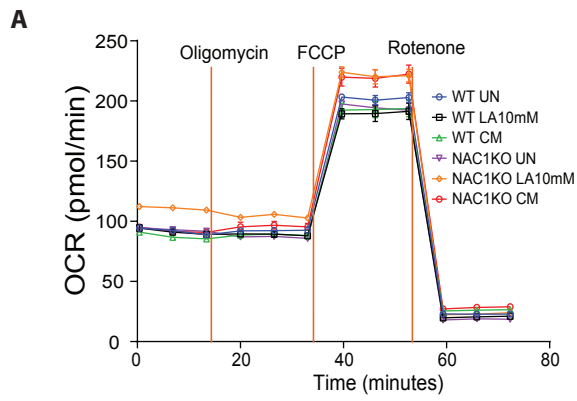
711 **Figure 7. NAC1 KO Tregs support tumor growth.** Three million Tregs were *i.p.* injected in
712 each of the recipient Thy1.1⁺ congenic mice, followed by tumor engraftment. **(A)** Schematic
713 representation of adoptive Treg transfer and tumor engraftment. **(B)** Tumor growth curve of
714 B16F10 melanoma (n=5). **(C)** Representative survival curve. **(D)** Illustration of the proposed and
715 the rationale pathway regulated by NAC1-FoxP3, leading to mitochondrial fitness in the TME.

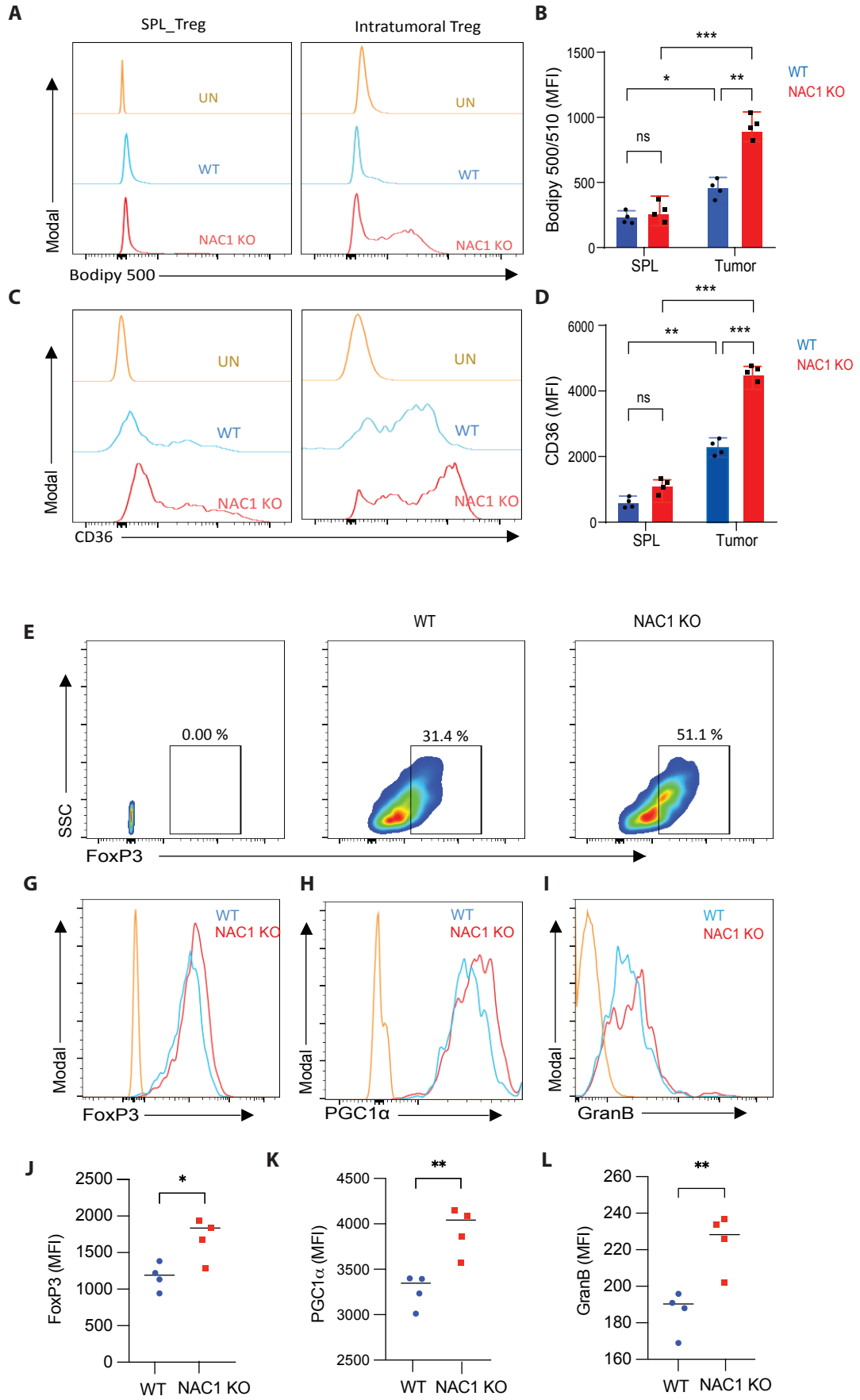


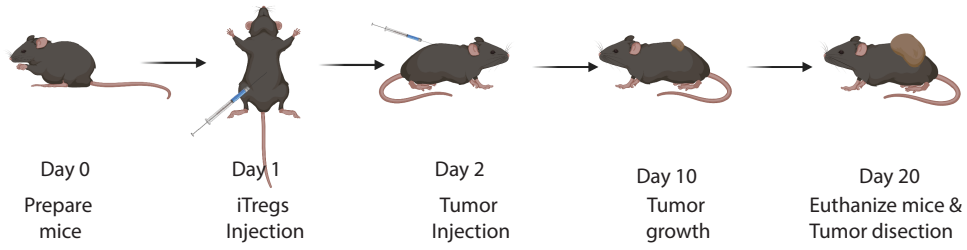
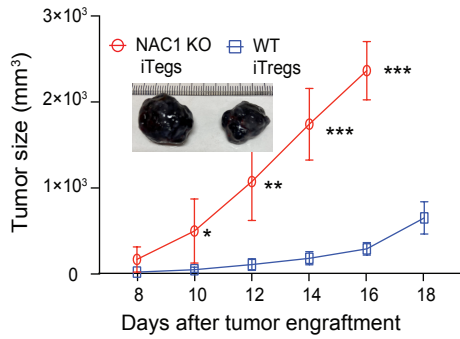
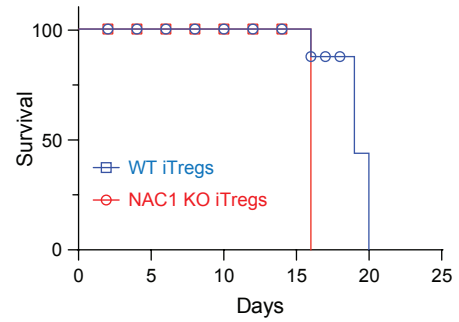










A**B****C****D**